



Compression Behavior and Impact Energy Absorption Characteristics of 3D Printed Polymer Lattices and Their Hybrid Sandwich Structures

Xia Zhou, Chi Qu, Yan Luo, Roger Heise, and George Bao

Submitted: 17 December 2020 / Revised: 30 July 2021 / Accepted: 3 September 2021 / Published online: 22 September 2021

In this paper, the compression behavior of four lattice topologies with body-centered and face-centered structures was first analyzed numerically based on the material model of 3D printed polylactic acid (PLA). To enhance the interface bonding properties between the AZ31B Mg face sheets and the PLA lattice cores, the skin-core interface was preprocessed by 3D printing microgrooves on PLA pre-pregs. The interface parameters of the heterogeneous bonding layer were then obtained through DCB and ENF experiments. The impact simulation by using ABAQUS/Explicit with a self-written VUMAT subroutine for the enhanced interfacial layer was finally carried out for the hybrid Mg alloy skin and PLA lattice-core sandwich panels with high energy absorption characteristics under static compression. The results have shown that the BCCZ and F₂CCZ lattice configurations with Z-direction pillars exhibit better quasi-static compression characteristics compared with the BCC and F₂CC structures. Interlayer fracture toughness values G_{IC} and G_{IIC} of the skin-core interface can reach up to 0.63 and 7.02 kJ/m², respectively. Under low-velocity impact, the hybrid sandwich panels with F₂CCZ lattice cores exhibit better impact resistance and energy absorption capacity than those of the BCCZ lattice sandwich panels.

Keywords compression behavior, hybrid sandwich structures, impact energy absorption, PLA lattice configuration, VUMAT subroutine

1. Introduction

3D printing of polymer and polymer composites has achieved remarkable achievements so far (Ref 1, 2), while novel hybrid composite sandwich panels combining 3D printed lattice cores and different facing materials have a wide application prospect due to their obvious advantages such as lightweight, multi-functional performance, design flexibility (Ref 3-5). For novel hybrid sandwich panels typically composed of lightweight metal or carbon fiber polymer composite (CFRP) face sheets and 3D printed polymer or metal lattice cores, 3D printed polymer lattice cores are characterized by easy preparation process, fewer defects, and more stable performance compared with metallic lattice structures (Ref 6), but mechanical properties of these hybrid structures are affected to

a great extent by the lattice core configuration, the face-core interface, and different facing and core material characteristics (Ref 7). Therefore, the research on mechanical properties of 3D printed polymer lattice core of different configurations and their hybrid sandwich structures with magnesium alloy face sheets have both theoretical significance and practical application value.

Compression and impact energy absorption characteristics are important mechanical properties of lightweight sandwich structures. Traditional magnesium alloy based hybrid sandwich panels with 2D carbon fiber reinforced polymers (CFRP) cores have been shown to possess good mechanical and acoustic as well as energy-absorbing properties et al. (Ref 8-11), but the effects of 3D printed polymer or CFRP lattice cores and their topologies on the compression behavior and energy absorption characteristics of lightweight metal-polymer hybrid sandwich structures are rarely reported (Ref 12). In recent years, the research work on polymer lattice cores by FDM 3D printing has been gradually carried out due to their lightweight, processing flexibility, and parameters-insensitive properties. Some researchers (Ref 12-15) have investigated the compressive behavior and low-velocity impact response of the 3D printed single polymer lattices or their sandwich structures with different lattice core topologies and relative densities both experimentally and numerically. Some other researchers (Ref 16, 17) proposed novel hybrid techniques based on additive manufacturing and materials joining principles for layered metal-polymer hybrid structures under tensile and quasi-static loading. However, the existing researches are mainly focused on static and dynamic mechanical properties of a single polymer lattice core, and a few research is reported on mechanical properties of hybrid metal-polymer sandwich structure due to weak dissimilar interface bonding.

In the present paper, the numerical analyses on the quasi-static compressive behavior of 3D printed polylactic acid (PLA)

This invited article is part of a special topical focus in the *Journal of Materials Engineering and Performance* on Additive Manufacturing. The issue was organized by Dr. William Frazier, Pilgrim Consulting, LLC; Mr. Rick Russell, NASA; Dr. Yan Lu, NIST; Dr. Brandon D. Ribic, America Makes; and Caroline Vail, NSWC Carderock.

Xia Zhou and **Yan Luo**, State Key Laboratory of Structural Analysis for Industrial Equipment, Department of Engineering Mechanics, Faculty of Vehicle Engineering and Mechanics, Dalian University of Technology, Dalian 116024, People's Republic of China; and **Chi Qu**, **Roger Heise**, and **George Bao**, Research and Development Division, Peninsula Alloy Inc., Stevensville, Canada. Contact e-mail: zhouxia@dlut.edu.cn.

lattice structures of different configurations and relative densities were first conducted. Numerical predictions for the quasi-static compression of different lattice configurations were then compared. In addition, the interface parameters of the enhanced skin-core bonding layer by 3D printing microgrooves on PLA pre-pregs were obtained through DCB and ENF experiments. Simulation study on the low-velocity impact response of composite sandwich panels with hybrid AZ31B Mg skin and optimized polymer lattice cores were finally carried out by using ABAQUS/Explicit with a self-written VUMAT subroutine for the interfacial layer. The results of the study will provide a reference for the prediction and optimization of the

mechanical properties of advanced metal/polymer hybrid structures.

2. Materials and Methods

2.1 Sample Preparation and Mechanical Testing

Figure 1 shows the typical Body-Centered Cubic (BCC) micro lattice sandwich structure with AZ31B Mg alloy face sheets and 3D printed PLA lattice cores. PLA lattice cores were printed by using Fused deposition modeling (FDM) technology and modified PLA filaments purchased from Hangzhou Zhuopu New Material Technology Co., Ltd., China. The print parameters are shown in Table 1. The face sheet and lattice core were adhesively bonded by thermosetting two-component epoxy resin and then placed into the curing mold under a specific pressure. In order to improve the interface bonding strength, the PLA lattice cores with microgroove patterns of PLA skins (1.6 mm) were printed before preparation of the hybrid sandwich panel.

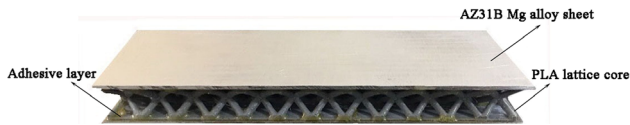


Fig. 1 Experimental preparation of the hybrid sandwich panel with BCC lattice core

Table 1 Printing parameters for modified polylactic acid materials

Layer thickness, mm	Temperature, °C		Printing speed, mm/s	Material filling rate, %
	Extrusion	Bed		
0.19	230	60-70	30	100

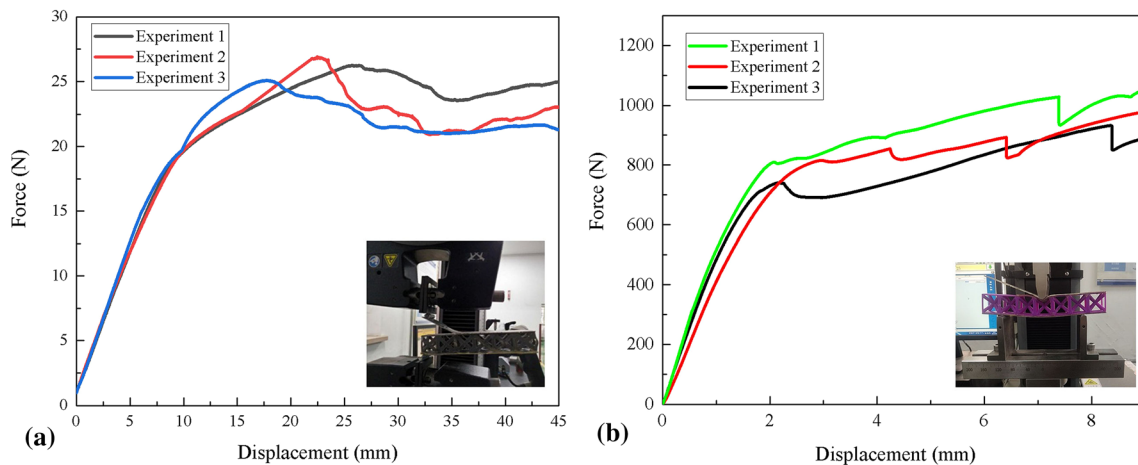


Fig. 2 Typical load-displacement curves obtained by (a) DCB and (b) 3ENF tests for the hybrid sandwich panel

Table 2 Parameters of four lattice cellular unit cell configurations

Relative density ($\bar{\rho}$), %	Strut diameter d , mm				Length of cell side L , mm
	BCC	BCCZ	F ₂ CC	F ₂ CCZ	
10	3.49	3.27	3.89	3.62	24
15	4.36	4.08	4.87	4.54	
20	5.12	4.80	5.73	5.37	

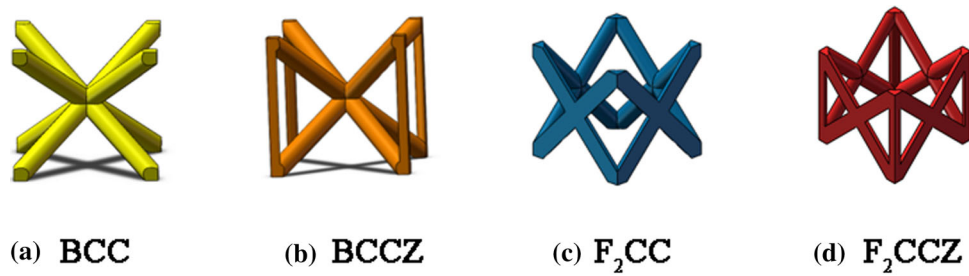


Fig. 3 Body-centered cubic and face-centered cubic as well as their derived lattice cells

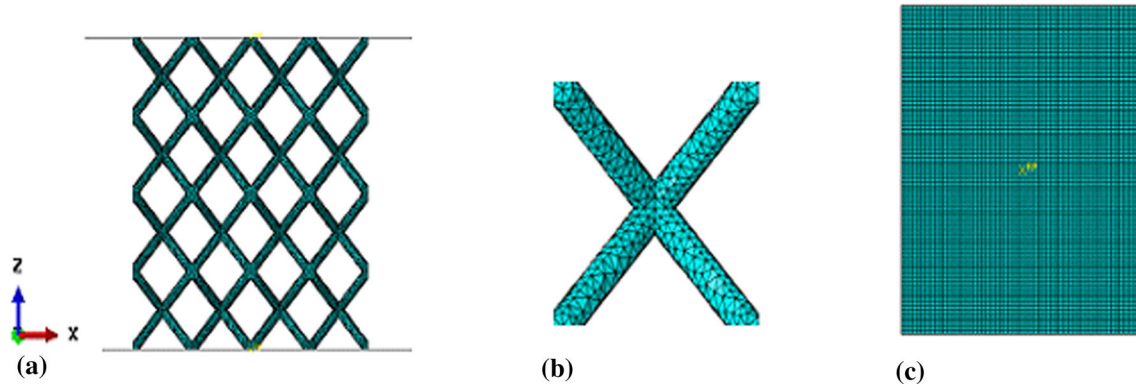


Fig. 4 (a) BCC lattice compression model, (b) FE mesh of the unit cell, and (c) FE mesh of the indenter

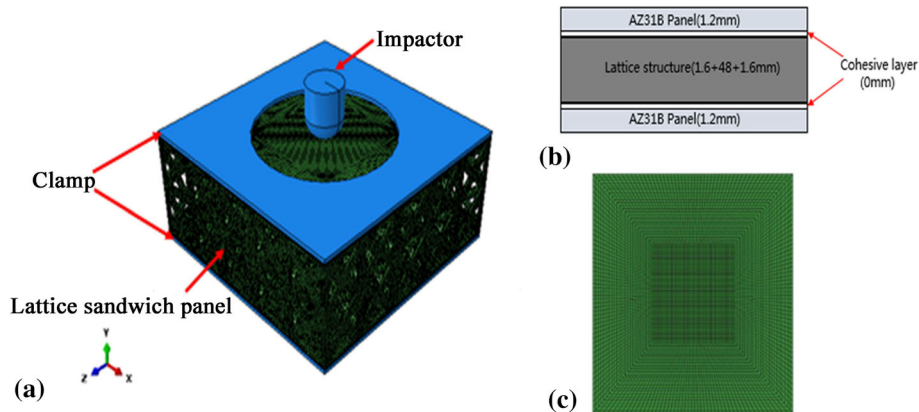


Fig. 5 (a) Drop weight impact model and (b) schematic diagram for hybrid lattice sandwich panel as well as (c) FE mesh of the face sheet

The fracture toughness of the skin-core interface with 3D printed microgrooves was investigated using the Mode-I and Mode-II tests of the sandwich panel at room temperature. Mode I interlaminar fracture toughness of the sandwich panel was measured according to the ASTM 5288-2013 standard using the double cantilever beam (DCB) specimen with length of 144 mm, width of 24 mm, thickness of 29.6 mm (including Mg face sheet) and pre-initial crack length of 50 mm. Mode-II tests of the sandwich panel were conducted according to the ASTM D7905/D7905M-14 standard using the end-notch flexure (ENF) specimen. The specimens used are 138 mm in span length, 24 mm in width, 29.6 mm in thickness, and 50 mm in pre-initial crack length. The mode I and mode II fracture toughness values of the skin-core interface were calculated from the load-displacement curves (Fig. 2) and they

were 0.63 and 7.02 kJ/m², respectively. The normal and shear strength of the adhesive layer are 18 and 31 MPa, respectively (Ref 18).

2.2 Finite Element Modeling

Four lattice core structures including BCC, BCCZ, F₂CC, and F₂CCZ lattices were designed in this paper, as shown in Fig. 3. For convenience of comparison, these lattice unit-cells are designed to have the same unit-cell side length L but different relative densities $\bar{\rho}$.

The specific dimensions of each lattice unit cell with three relative densities $\bar{\rho}$ are shown in Table 2. The relative density is adjusted by varying the strut diameter d while keeping all other parameters constant.

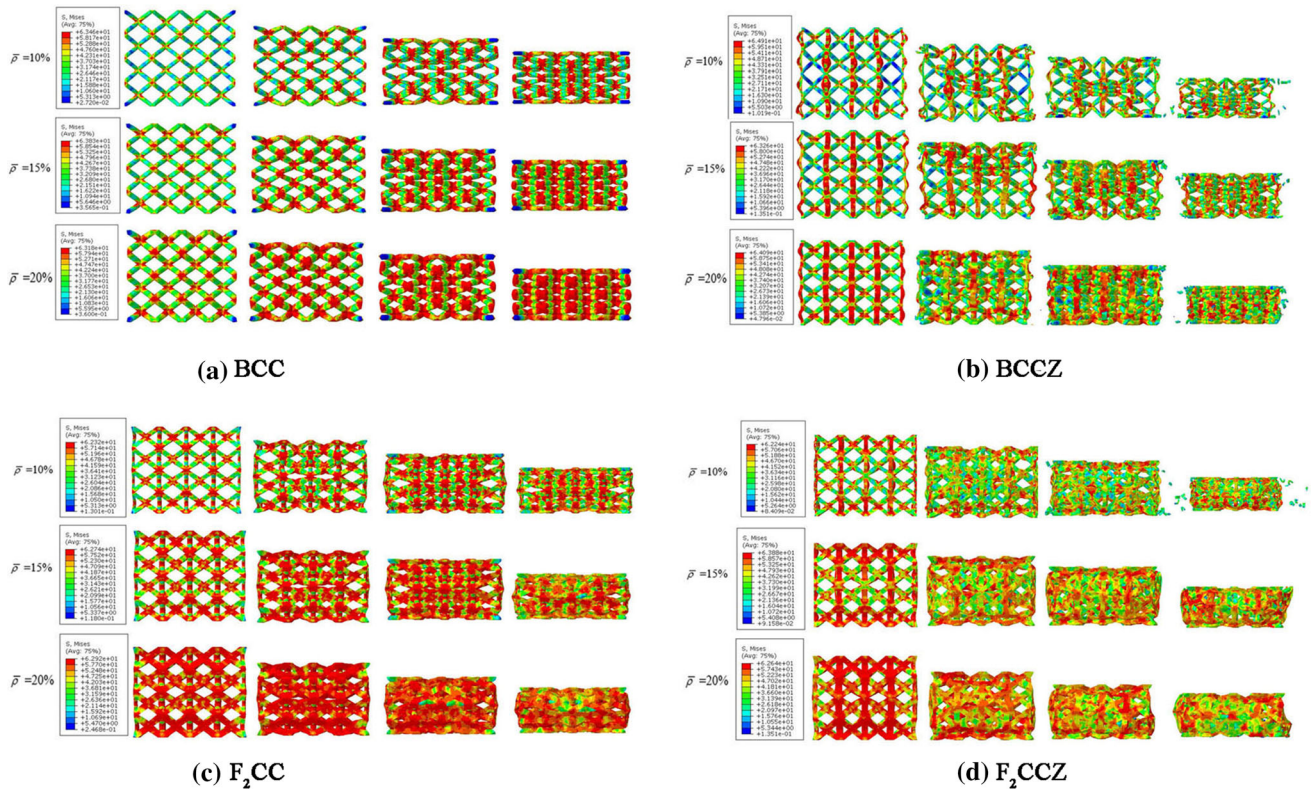


Fig. 6 The contours of the von Mises stress for different lattice structures with various relative densities

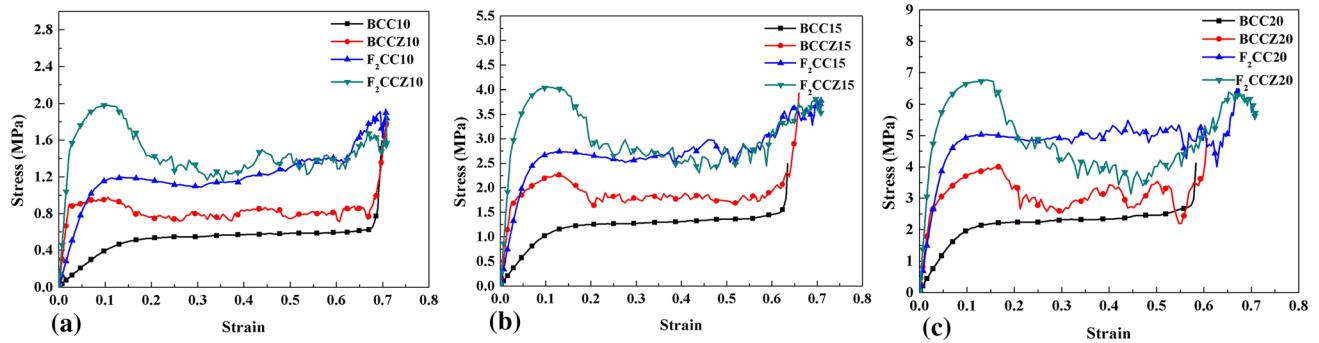


Fig. 7 Comparison of compressive stress-strain curves for different lattice structures of (a) 10%, (b) 15% and (c) 20% relative density. Here, BCC10 denotes the BCC lattice with relative density of 10%, and so on for other symbols.

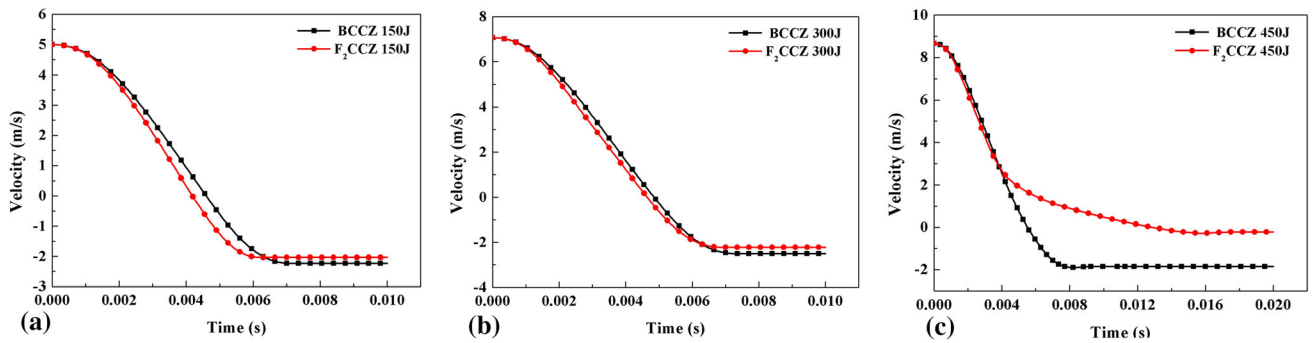


Fig. 8 Velocity versus time curves of BCCZ and F₂CCZ lattice sandwich panels under different impact energies

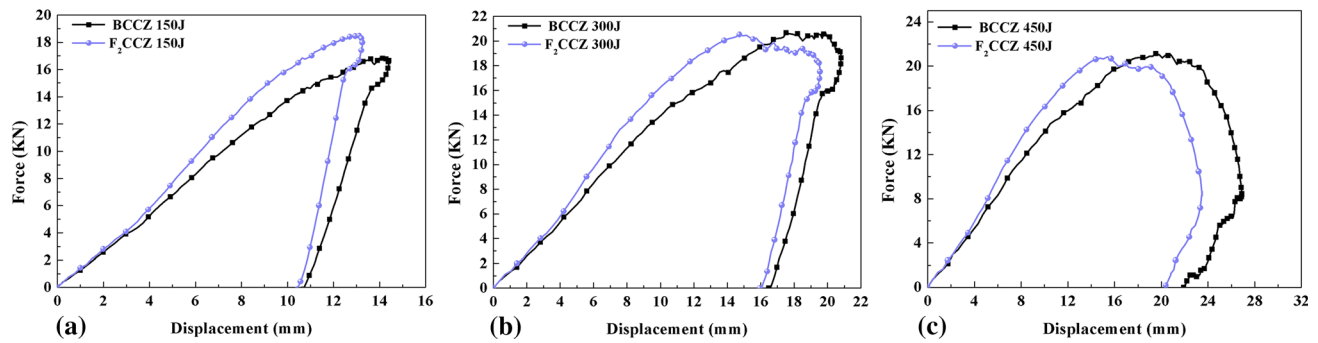


Fig. 9 Force versus displacement curves of BCCZ and F_2CCZ lattice sandwich panels under different impact energies

Numerical simulation of compressive behavior and low-velocity impact response was performed in Abaqus/Explicit by using a three-dimensional finite element analysis model. Figure 4 shows the finite element mesh model (containing $4 \times 4 \times 4$ unit cells) for compressive behavior analysis of the typical BCC lattice with 10% relative density. In the compressive model, four-node stiffness units (R3D4) and the default mesh size 7 mm are used for the upper and lower rigid surfaces, while the lattice core is discretized by C3D4 element and the optimal element size is about 1.2 mm by the mesh convergence test. In addition, reference points are defined on the upper and lower rigid surfaces, and coupling constraints are set with the rigid surfaces. The default hard contact is used for the normal behavior and the friction coefficient between the contact surfaces is 0.2, and the reference points coupled with the rigid surfaces are completely fixed. A smooth step curve is used for displacement loading. The indenter moved only along the compression direction, and the displacement constraints are applied in other directions.

Figure 5 shows the finite element mesh model (containing $5 \times 5 \times 2$ unit cells) for drop weight impact analysis of the BCC lattice with 15% relative density in which a more refined mesh is defined in the central zone of the impactor. The Mg alloy face-sheets and the lattice core layers with a PLA thin panel by an integrated FDM printing were both meshed using 3-D solid elements in which the linear hexahedral elements of type C3D8R are used for the former and the tetrahedron elements of type C3D10M are used for the latter. The adhesive layers with enhanced interface parameters between the two are simulated by zero-thickness cohesive elements of type COH3D8 due to the existence of 3D printing microgrooves. For medium and high-energy drop weight impact (150–450 J), the rigid impactor has a hemispherical head of 10 mm radius and a fixed mass of 12 kg, and rigid body constraint is applied to the coupling point; while for the low-velocity impact using split Hopkinson pressure bar (SHPB), the long rod piercing bullet is used to avoid the edge effect. The steel long rod bullet has the size of $\Phi 22.37 \times 400$ mm, and the impact speed is 22.83 m/s.

To model compressive behavior and low-velocity impact response of the novel hybrid sandwich panels, the modified Mazars damage model (Ref 19) by introducing an expression for damage variable for 3D printed PLA core layers are implemented by developing finite element codes using ABAQUS/Explicit with a self-written user-defined subroutine (VUMAT) and the maximum equivalent plastic strain criterion is adopted for element failure, while the interface delamination is simulated by an exponential cohesive zone model implemented into user subroutines in ABAQUS and the mechanical

properties of magnesium alloy layers are described using the Johnson-Cook model (Ref 20). All the other parameters (including parameters of adhesive layers and 3D printed PLA materials) used in the simulation model are inputted based on the experimental results from Fig. 2 and in reference (Ref 19). To validate the correctness of the simulation method, the simulation predictions are compared with experimental results based on SHPB tests.

3. Results and Discussion

3.1 Compressive Failure Mode in FDM Lattice Structures

Figure 6 shows comparison of the von Mises stress contours of different lattice structures in the typical stages (elastic-plastic deformation, yield platform, densification) of the compression process. It can be found that there exists approximately the same distribution of the equivalent stress for the same lattice configuration with different relative densities. The stress distribution is symmetrical with respect to the lattice center and the stresses in the struts (BCCZ and F_2CCZ lattice) or in the nodes (BCC and F_2CC lattice) are the greatest. However, the stress distributions for the BCCZ and F_2CCZ lattice structures with different relative densities are more homogeneous than for the BCC and F_2CC lattice structures as the struts in orientation-Z are subjected to major compression loads.

In addition, compared with the BCC and F_2CC lattice structures, similar failure modes such as fracture of nodes, buckling of struts and local collapse of cores may occur in the BCCZ and F_2CCZ lattice structures during the compression process, but their compression-failure resistance has been improved with the increase in the relative density of lattice structures (10 to 20%). By further comparing the BCCZ and F_2CCZ lattice structures, it can be found that with increasing relative densities of lattice structures, the failure of inclined section truss of the latter leads to its overall collapse failure and the decreased bearing capacity.

3.2 Compressive Bearing Capacity of Lattice Structures

The compressive stress-strain curves of the four lattice structures are shown in Fig. 7. It can be seen that for the same lattice configuration, the compressive modulus and yield strength increase with the increasing relative density while the densification strain decreases. For the four lattices with different relative densities, the hybrid sandwich structures with the BCCZ and F_2CCZ lattice cores both have larger equivalent

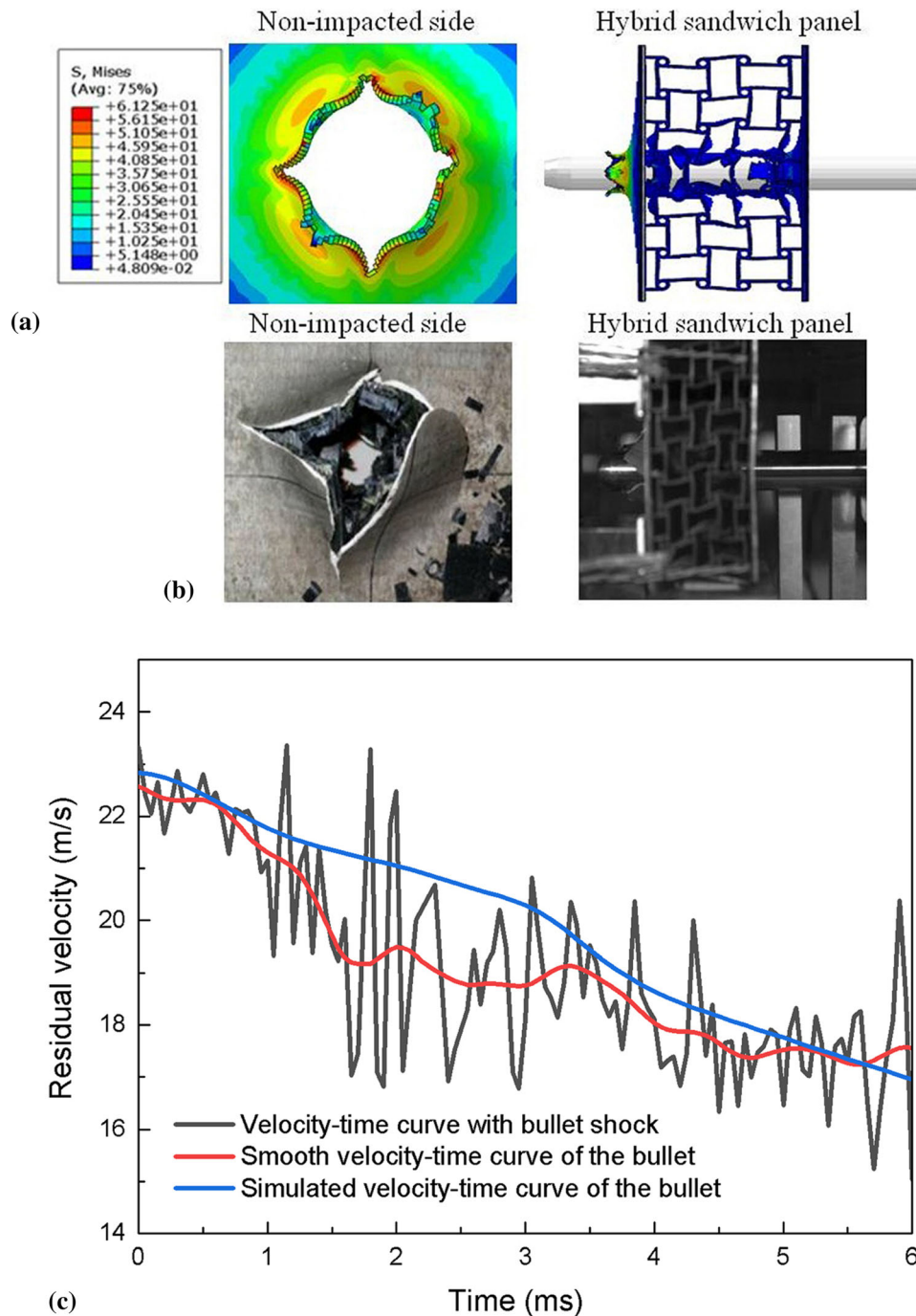


Fig. 10 Comparison of simulation predictions and experiment results: damage morphologies of non-impacted side and hybrid sandwich panel obtained by (a) simulation and (b) experiment, and residual velocity vs. time curves by (c) simulation and experiment

elastic modulus, yield strength, and densification strain than the other two lattice sandwich structures. In addition, the F_2CCZ lattice sandwich panel has a higher compressive mechanical performance than the BCCZ lattice sandwich panel under lower lattice relative density conditions (10-15%).

3.3 Impact Energy Absorption Characteristics of Hybrid Sandwich Structures and Validation of Simulation Models

Figure 8 shows the velocity-time history curve of the BCCZ and F_2CCZ hybrid sandwich panel with relative density of 20%

at different impact energies. Compared with the BCCZ lattice cores, F_2CCZ lattice sandwich panel has a lower residual velocity after impact, indicating better energy absorption capacity. Moreover, the F_2CCZ lattice sandwich panel has enhanced energy absorption characteristics than the BCCZ lattice sandwich panel with the increase of impact energy. In addition to the lattice core configuration, the face-sheet and interface adhesive layer also have an important impact on the impact resistance and energy absorption characteristics of the hybrid sandwich panel.

Figure 9 shows comparison of the impact force-displacement curves of the above two-hybrid sandwich panels with

BCCZ and F₂CCZ lattice cores at different impact energies. The peak impact force for the F₂CCZ lattice sandwich panel is higher when the impact energy is lower. However, the difference between the two kinds of lattice sandwich panels decreases with the increase of impact energy. The maximum penetration displacement for the BCCZ lattice sandwich panel at higher impact energy is larger, indicating that it has a longer buffering process and impact resistance.

To verify the correctness of the simulation models, the impact response and failure mode of the tetrachiral honeycomb core/AZ31 Mg face sheet hybrid sandwich structure with the overall size of 120 × 120 × 58 mm under low-velocity projectile impact loading were studied experimentally and numerically by using split Hopkinson pressure bar (SHPB) systems. Figure 10(a) and (b) shows comparison of the damage morphology and residual velocity versus time curve between numerical predictions and experimental results when the projectile velocity was 22.83 m/s. It can be seen from the simulation results that there are petal-shaped projections present on the non-impacted sides of the hybrid panel and Mg alloy layers due to the crack development and a large stress distribution appear at the edge of the crack tips (Fig. 10a and b). It can also be found that the damage and failure for the adhesive layer and PLA core mainly occur near the contact area between the impactor and the upper face sheet. The simulated damage morphology (Fig. 10a) is close to those obtained by experiments (Fig. 10b). In addition, as can be seen from Fig. 10(c), the simulated residual velocity curve is also close to the experimental curve. After the hybrid sandwich panel was subjected to impact, it still had a relatively complete shape, showing better low-speed projectile impact resistance.

4. Conclusions

From the research on the compressive behavior and impact energy absorption characteristics of novel hybrid sandwich panels, the following two conclusions are derived:

- (1) The BCCZ and F₂CCZ lattice structures exhibit improved compressive properties in load-bearing capacity, flexural stiffness, and strength, as well as energy absorption capacity compared with the BCC lattice structure. Moreover, the energy absorption characteristics of different lattice structures are enhanced in the order of the BCC, BCCZ, F₂CC, and F₂CCZ lattice structures under the same relative density conditions.
- (2) Within the range of impact energy considered in the present study (150 to 400 J), the hybrid sandwich composite panels with the BCCZ and F₂CCZ lattice cores exhibit different dynamic response characteristics. The BCC lattice sandwich panel has better impact resistance than the F₂CCZ lattice sandwich panel at high impact energy, while the F₂CCZ lattice sandwich panel has better impact resistance at low impact energy and higher impact energy absorption at high impact energy. This can be attributed to the synergistic effects of lattice core, enhanced skin-core interface, and Mg alloy face sheet under different impact energies. The consistency between simulation and experimental results for low-veloc-

ity projectile impact of hybrid sandwich panel validates the correctness of the simulation model.

Conflict of interest

The authors declared that there is no conflict of interest.

References

1. S. Bhandari and R. Lopez-Anido, Finite Element Analysis of Thermoplastic Polymer Extrusion 3D Printed Material for Mechanical Property Prediction, *Addit. Manuf.*, 2018, **22**, p 187–196
2. Y.K. Ming, S.Q. Zhang, W. Han et al., Investigation on Process Parameters of 3D Printed Continuous Carbon Fiber-Reinforced Thermosetting Epoxy Composites, *Addit. Manuf.*, 2020, **33**, p 101184
3. T.A. Schaedler, C.J. Ro, A.E. Sorensen et al., Designing Metallic Microlattices for Energy Absorber Applications, *Adv. Eng. Mater.*, 2014, **16**, p 276–283
4. T.A. Schaedler and W.B. Carter, Architected Cellular Materials, *Annu. Rev. Mater. Res.*, 2016, **46**, p 187–210
5. H. Yazdani Sarvestani, A.H. Akbarzadeh, H. Niknama et al., 3D Printed Architected Polymeric Sandwich Panels: Energy Absorption and Structural Performance, *Compos. Struct.*, 2018, **200**, p 886–909
6. T.Y. Yao, J. Ye, Z.C. Deng et al., Tensile Failure Strength and Separation Angle of FDM 3D Printing PLA Material: Experimental and Theoretical Analyses, *Compos. Part B*, 2020, **188**, p 107894
7. B. Han, Z.J. Zhang, Q.C. Zhang et al., Recent Advances in Hybrid Lattice-Cored Sandwiches for Enhanced Multifunctional Performance, *Extreme Mech. Lett.*, 2017, **10**, p 58–69
8. P.P. Zhou, X. Wu, Y.C. Pan et al., Mechanical Properties of Carbon Fibre-Reinforced Polymer/Magnesium Alloy Hybrid Laminates, *Mater. Res. Express*, 2018, **5**(4), p 046523
9. Y.C. Pan, G.Q. Wu, X. Cheng et al., Mode I and Mode II Interlaminar Fracture Toughness of CFRP/Magnesium Alloys Hybrid Laminates, *Compos. Interface*, 2016, **23**, p 453–465
10. X. Zhou, K. Li, C.H. Chen and X.C. Chen, Low-Velocity Impact Response and Damage Simulation of Fiber/Magnesium Alloy Composite Laminates, *J. Vib. Shock*, 2018, **37**(22), p 1–9. ((in Chinese))
11. D. De Cicco and F. Taheri, Performances of Magnesium- and Steel-Based 3D Fiber-Metal Laminates under Various Loading Conditions, *Compos. Struct.*, 2019, **229**, p 111390
12. Z.B. Liu, H.T. Chen and S.Q. Xing, Mechanical Performances of Metal-Polymer Sandwich Structures with 3D-printed Lattice Cores Subjected to Bending Load, *Arch. Civ. Mech. Eng.*, 2020, **20**, p 89
13. L. Chen, C. Alessandro, D.G. Michael and C. Philip, Mechanical Behaviour of Additively-Manufactured Polymeric Octet-truss Lattice Structures under Quasi-static and Dynamic Compressive Loading, *Mater. Des.*, 2019, **162**, p 106–118
14. W.F. Liu, H.W. Song, Z. Wang, J.T. Wang and C.G. Huang, Improving Mechanical Performance of Fused Deposition Modeling Lattice Structures by a Snap-Fitting Method, *Mater. Des.*, 2019, **181**, p 108065
15. A.J. Turner, M. Al Rifaie, A. Mian and R. Srinivasan, Low-Velocity Impact Behavior of Sandwich Structures with Additively Manufactured Polymer Lattice Cores, *J. Mater. Eng. Perform.*, 2018, **27**, p 2505–2512
16. R. Falck, S.M. Goushegir, J.F. dos Santos and S.T. Amancio-Filho, AddJoining: A Novel Additive Manufacturing Approach for Layered Metal-Polymer Hybrid Structures, *Mater. Lett.*, 2018, **217**, p 211–214
17. J. Butt and H. Shirvani, Experimental Analysis of Metal/Plastic Composites Made by a New Hybrid Method, *Addit. Manuf.*, 2018, **22**, p 216–222
18. X. Zhou, Y.T. Zhao, X.C. Chen, Z.F. Liu, J.L. Li and Y.F. Fan, Fabrication and Mechanical Properties of Novel CFRP/Mg Alloy Hybrid Laminates with Enhanced Interface Adhesion, *Mater. Des.*, 2021, **197**, p 109251
19. X. Zhou, J.L. Li, C. Qu, W.M. Bu, Z.F. Liu, Y.F. Fan and G. Bao, Bending Behavior of Hybrid Sandwich Composite Structures Containing 3D Printed PLA Lattice Cores and Magnesium Alloy Face

Sheets, *J. Adhes.*, 2021 <https://doi.org/10.1080/00218464.2021.1939015>

20. F. Feng, S. Huang, Z. Meng et al., A Constitutive and Fracture Model for AZ31B Magnesium Alloy in the Tensile State, *Mat. Sci. Eng. A Struct.*, 2014, **594**, p 334–343

Publisher's Note Springer Nature remains neutral with regard to jurisdictional claims in published maps and institutional affiliations.